Measurements of velocity fields in internal gravity waves. Documentation of experimental method

by

J. Kristian Sveen, Atle Jensen and John Grue

Mechanics Division, Department of mathematics,
University of Oslo, Norway

Abstract

This paper concerns experimental measurements of internal gravity waves in a two-fluid system with fresh water above salt water, and acts as a complement to an article by Grue, Jensen, Rusås and Sveen (1998). We investigate properties of these waves such as velocity field, propagation speed and wave shape comparing with fully nonlinear theory. To measure these quantities we have applied Particle Tracking Velocimetry (PTV), finding that this method is particularly useful in our experiments due to the relatively small velocities and accelerations induced by the waves. The wave amplitudes, nondimensionalized by the depth of the thinner layer, range from 0.22 up to 1.5, the latter being slightly less than the theoretical maximum. The thickness of the pycnocline is on the order of 0.13-0.26 times the upper layer thickness. We generate solitary waves by releasing a volume of fresh water trapped behind a gate and we focus on initial conditions resulting in a single solitary wave. The error in the measured velocities nondimensionalized by the linear long wave speed is less than about 7-8%.

This paper contains a full description of the experimental setup and method, and complements the article by Grue et al. (1998), where all these details could not be included. We have in this paper included some of the results obtained for visualization purposes, but a complete presentation of the results, including comparison with both fully nonlinear and weakly nonlinear theories, can be found in the article mentioned above.

1 Introduction

In the recent years the experimental methods for investigating fluid flows have been increasing in parallel to the availability and the increase of computer power. Especially non-intrusive techniques like Particle Tracking Velocimetry (PTV) and Particle Image Velocimetry (PIV) have been subject to a lot of development over the last decade. Both of these methods use tracer particles and measure the velocity of these particles, and they both have the obvious advantage of measuring a full velocity field in a two-dimensional slice of a flow. The two methods differ in the way that the velocities are obtained. PIV is based on tracking ensembles of particles between (usually) two images, using the correlation function (cross correlation or auto correlation) giving the displacement, δx, from the first to the second image. Dividing by the time between the images, Δt, gives the velocity. PTV, on the other hand, relies on tracking individual particles in images, usually over longer time sequences. The advantage of PTV compared to PIV is that commercially available PTV systems are relatively cheap compared to the PIV systems, and also that it gives a lagrangian view of the flow. Both methods are quite accurate, with PIV being the better of the two. For more information about these methods see e.g. Adrian (1991).

The PTV software program we have available also provides us with the possibility of image analysis and flow visualization. We have used this part of the program to quite accurately measure the wave shape and propagation speed.

Several authors have made an experimental investigation of internal waves and compared the results with theory. Koop and Butler (1981) described the shape, wavelength and the amplitude of solitary waves. They used Korteweg-de Vries (KdV) theory (Long 1956), finite-depth theory and the Benjamin-Ono theory. They concluded that there was good agreement between the experiments and the KdV theory, but they did not find a good comparison with finite-depth theory and the Benjamin-Ono theory. Kao, Pan and Renouard (1985) also made an experimental analysis of internal waves and they found good agreement between experimental results and KdV theory, even for rather large amplitudes.

The motivation for this paper is to make a detailed description of the PTV method, the software and the experimental setup, in such a way that it complements the paper by Grue et al. (1998). The purpose of the experiments is to make a general analysis of the internal solitary waves and compare these results with theory. The results for wave shapes have been omitted here but is included in the paper mentioned above.

Following the introduction we describe in section 2 in detail the experimental method and procedure. In section 3 we show some of the results from our investigation of velocity fields and propagation velocity. Finally, section 4 is a conclusion.

2 Experimental setup

2.1 Wave tank

The experiments described in this paper are undertaken in a wave tank of 25 m length, where usually two different sections of 6.2 m and 12.3 m length have been used. On one occasion we also used a tank length of 21.5 m. The tank is 0.50 m wide, approximately 1 m deep and with walls and bottom made of glass. At one end of the tank we installed a removable gate of the same width as the tank, which functioned as the wave generator, and at the other end we used a reflecting wall. Waves are generated by trapping a pool of light water behind the gate, whereby the gate can be lifted to allow the rectangular initial volume to propagate downstream. A schematic view of the wave tank is shown in figure 1.

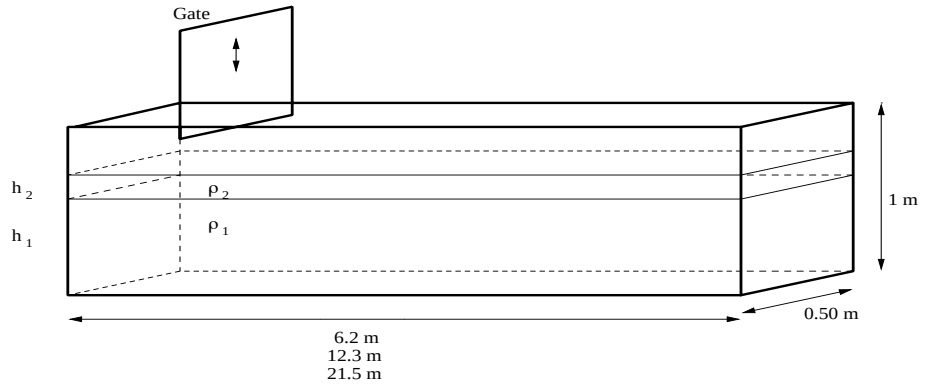

Figure 1: Schematic view of the wave tank.

2.2 Recording equipment and software

The experiments are recorded by two COHU 4912 standard monochrome CCD cameras onto a video-recorder, through a multiplexer, with a resolution of 560×575 pixels (horizontal times vertical). The cameras are positioned approximately 2.2 m away from the tank wall with the first camera located about 4.15 m from the upper end of the tank and the cameras 5.927 m apart. Only the first of these camera positions were used during the experiments with the shortest wave tank.

The recordings are analysed by the software program DigImage which is developed and described in Dalziel (1992 §3). DigImage is made to run on standard IBM compatible PC systems, with a Panasonic AG7350 Super VHS video-recorder. The computer controls the video recorder through a modified RS232 interface and grabs images using a Data Translation DT-2862 Frame Grabber card. The latter digitizes images with a resolution of 512×512 pixels in 256 grey levels, using the middle 512 pixel rows in both directions of the images (560×575 pixels). The computer also controls a DT 2859 multiplexer that

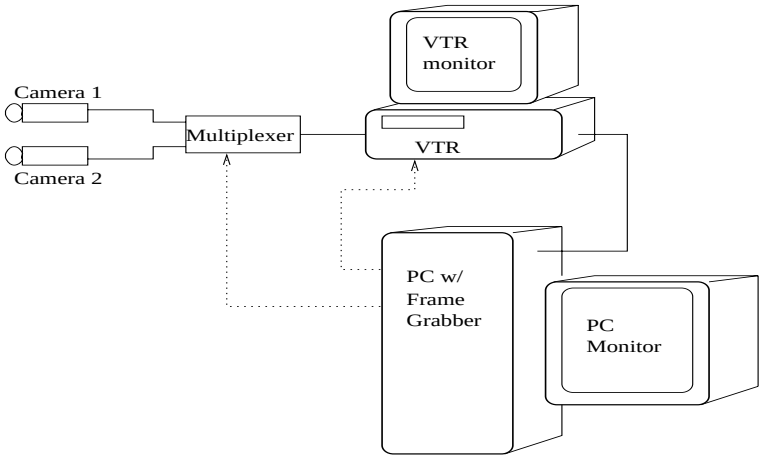

Figure 2: Schematic view of the technical equipment.

allows DigImage to switch between the two cameras. Figure 2 shows a schematic view of the recording equipment and arrangement.

2.3 Calibration of a two-layer fluid separated by a sharp pycnocline

A two-layer model with fresh water of density $\rho_2 \approx 0.999...$ kg/dm^3 on top of a lower layer of salt water of density $\rho_1 \approx 1.022...$ kg/dm^3 is calibrated. The upper layer, of thickness $h_2 = 0.15$ m, is slowly filled on top of the lower layer, of thickness $h_1 = 0.62$ m, through one (or in some cases two) floating sponges. In some experiments we have also used $h_1 = 0.31$ m and $h_2 = 0.15$ m. The filling of the wave tank alone may take up to 6 hours.

2.4 Density measurements

Density profiles are measured using a Yokogawa SC12 head probe conductivity meter. These measurements are supplemented by reference measurements of the density of the water at the surface and the brine at the bottom of the tank, using a Mettler Toledo DA-300M densitometer. The latter apparatus measures the density to four digits accuracy. With this setup we can easily measure the shape of the conductivity profile in a relatively fast manner and then match the upper and lower values of the conductivity meter to the reference density measurements. In this paper we have chosen to present the conductivity measurements as is. A typical conductivity measurement is presented in figure 3 with conductivity measured in mSiemens.

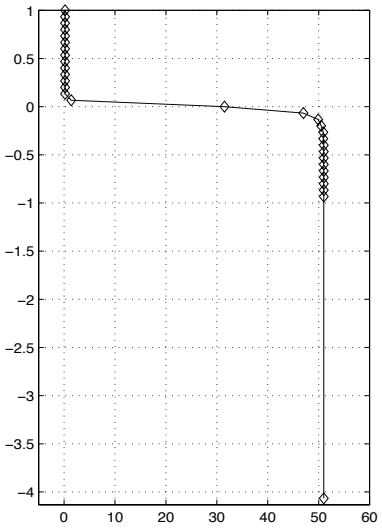

Figure 3: Typical conductivity profile with mSiemens on the horizontal axis and $\frac{y}{h_2}$ on the vertical axis.

2.5 Wave generation mechanism

Waves are generated by trapping a pool of light water behind the gate, whereby the gate can be lifted to allow the initial volume to propagate downstream. This generation procedure is similar to that of Kao et al. (1985), and is a robust method for generating solitary waves. In our experiments we have focused on initial conditions leading to a single solitary wave.

2.6 Particles

To obtain data from the experiments we add tracer particles that are assumed to closely follow the fluid flow. Results of an analysis of this aspect is given later in chapter 2.10. The particles used are Pliolite VTAC, a white colored resin used in the manufacture of paint. The particles are supplied in granular form and thereafter ground and sieved to obtain the desired size range. Pliolite VTAC have a specific gravity approximately equal to $\rho \approx 1.0228$ kg/dm^3, which is suitable in our experiments. Before adding the particles to the fluid it is necessary to soak them in wetting agent to remove the surface tension. We find that by soaking the particles for about 50 minutes in ordinary dishwasher wetting agent, most of the surface tension is removed resulting in particles approximately neutrally buoyant in the lower layer. Furthermore we find that by allowing some of the particles to soak for a shorter time we can leave some of the surface tension intact and thus allow small air bubbles to attach to the particles. By reducing the time to about 10-20 minutes a substantial amount of the particles become approximately neutrally buoyant in fresh water. Care is taken to ensure that all the wetting agent is washed off the particles before the experiments start.

2.7 Illumination

Illumination is provided by two powerful overhead projectors. Each is set to produce a sheet of light, approximately 5 cm wide, that is projected onto a mirror which reflects the sheets into the wave tank through the bottom. Care is taken to ensure that the sheet is parallel to the tank walls. The light sheet is centered 10 cm from the tank wall measuring into the tank. This setup is shown in figure 4.

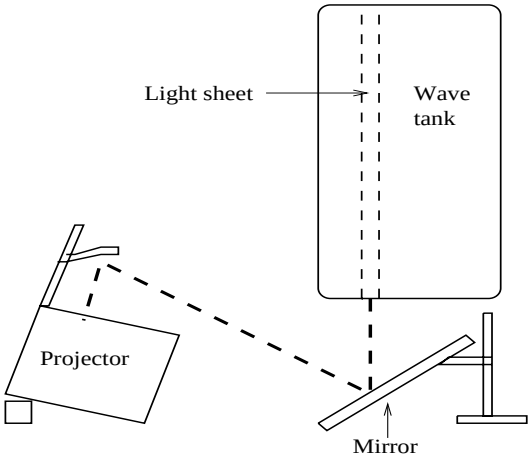

Figure 4: Schematic view of the illumination setup.

2.8 Velocity measurements

Particle Tracking Velocimetry (PTV) is a technique based on tracking individual particles over a certain time interval and then determining the particle velocities from their individual paths. The tracking process can be divided into 4 different tasks: 1) image acquisition, 2) locating particles, 3) tracking particles from one time step to the next and 4) subsequent analysis. In some cases it is possible and desirable to use image manipulation and enhancement prior to processing to improve the results. In these experiments we have focused on generating good quality images, and therefore no image enhancement is used.

2.8.1 Image acquisition

This part is already discussed in chapter 2.2. We record sections of the fluid, either 50×40 cm^2, 40×30 cm^2 or 80×60 cm^2, using mostly the former.

2.8.2 Locating particles in an image

Before tracking can take place a number of control parameters need to be defined in the DigImage program, including physical coordinate mapping, reference points and parameters concerning the particle images. The physical coordinate mapping is a question of

mapping the location of the particle on the video to its physical position in the experiment. This is accomplished by videoing a perspex plate with inscribed grid points, inserted into the light-plane of the tank after each experiment. These grid points mark what we denote by "world coordinates". We use an 8mm thick perspex plate with holes drilled half way through in a pattern defining the actual coordinate system. These holes have a diameter of 2.8mm and we use a center to center distance of 10 cm. After locating these world coordinate points on the video screen we need to define the mapping between the coordinate system in the video recording and the physical coordinate system. We have chosen to use a linear mapping function for this purpose.

In the mapping between the local coordinates and the world coordinates it is assumed that there is no translation (or rotation) from picture to picture. This is seldom the case, however, as the process of first recording and then grabbing (digitizing) the images may introduce small translations (and possibly rotations) as well as noise to the image in question. This "jitter" will generally be different from one image to another. To correct for this, and possibly vibrations of the camera, we use reference points along the right side of the viewed section. These reference points are positioned on the outer wall of the tank and consist of an electronic circuit board with nine LED's with adjustable intensity. The reference points are thereby introduced slightly out of the focal plane of the camera, but this is a negligible offset compared to the distance from the camera to the wave tank, which is not important in determining their individual positions. In each image the software program first locates particles in local pixel coordinates, then "jitter"-corrects and maps to reference coordinates and finally maps to the world coordinate system.

Particles are recognized in an image based on a set of criterions concerning the intensity, size and shape. To locate a particle we initially require that a region of an image, to be recognized as a blob, satisfies a spatially uniform threshold level. This region is then checked against the allowable limit on size, shape and intensity characteristics to determine if the blob should be considered a valid particle. In our experiments we use a lower threshold level of approximately 25 and an upper threshold of approximately 80. The lower limit on size is set to be a minimum of 3 pixels totally, with 2 pixels in both horizontal and vertical directions. A typical image of a particle in our experiments, however, is about 6-8 pixels large (see figure 5).

When a region of an image has been approved as a particle it is necessary to determine its exact physical position. In these experiments we use the centroid of a particles intensity to determine its position. This position is then checked against the centroid of the area to make sure that the difference between these methods does not exceed a predefined limit, typically less than one pixel. Figure 6 illustrates the procedure of determining the position. Dalziel (1992) estimated that a particle extending at least three pixels in both horizontal and vertical direction may typically be located to an accuracy of better than 0.2 pixels.

We note that the video cameras used in these experiments have an effective shutter speed of 3/100 s, thus allowing a particle moving with 10 cm/s, which is a typical maximal velocity in our experiments, to move a few (~ 3) pixels during exposure. This means that these particles will be somewhat larger than and also somewhat less bright than particles with lower speed. To some extent this explains why the particles in our experiments are

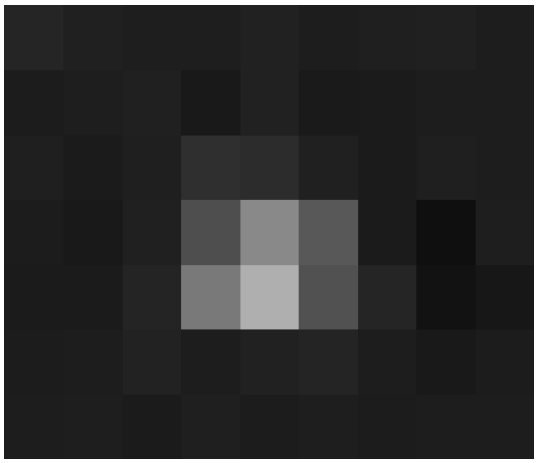

Figure 5: Typical particle image in our experiments. Each square equals to one pixel in the original image.

up to about 8 pixels large. It is possible to use a mechanical shutter with the cameras to reduce the shutter time but this will decrease the intensity in the images quite a bit and is therefore not used in these experiments.

2.8.3 Matching particles from one time step to the next.

Matching the particles from one time step to the next is described in depth by Dalziel (1992 §3.3 and §3.4). We shall here briefly outline the concept of matching particles between two successive time steps.

After we have found all particles in an image at time step $t = t_{n+1}$ we need to relate these back to the particles found at the previous time step to determine the individual paths. DigImage uses a method commonly referred to as the transportation algorithm (Hichcock (1941)), with some modifications. Potentially we can match any particle in the first image with any particle in the second or with the boundary. The matching with the boundary represents particles leaving or entering the light sheet implying that these particles have no matching particle. Some matches will always have a higher probability than others due to knowledge of the fluid flow, particle positions and particle characteristics. We therefore assign a cost to each possible particle to particle and particle to boundary association, depending on the previously mentioned parameters. The object of DigImage is then to minimize the cost of all associations to determine the optimal displacement.

2.8.4 Subsequent analysis

Having paired particles from one time step to the next we now want to calculate the velocities given all the particle positions at each time step. To do this we use the straight line fitted by least squares through five points in $x - t$ and $y - t$ space. This is illustrated

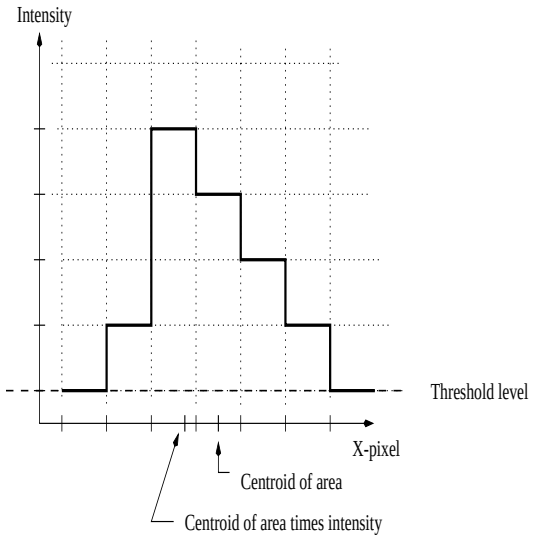

Figure 6: Centroid.

in figure 7. This means that we use the trace of the particles through 5 subsequent images with a separation of 0.04 s. If, for some reason, a particle has been tracked in less than 5 images, its path will not be used for a velocity calculation.

During these experiments we have on some occasions tracked more than 2800 particles, but the average experiment usually allows us to track between 800 and 2500.

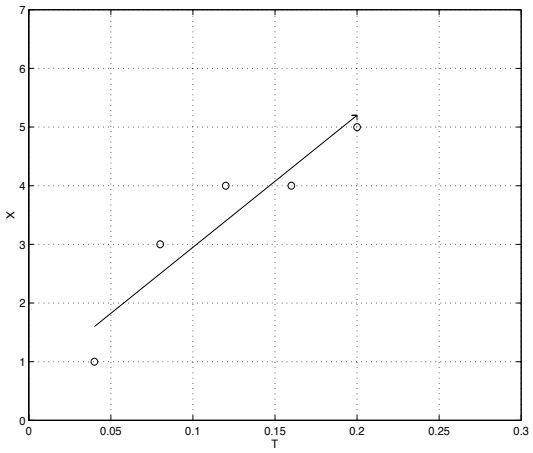

Figure 7: Least squares fit of a straight line to five points in $x - t$ space.

Due to the randomly located particles we need to define a grid to interpolate the individual particle velocities onto, before we can produce a vector plot of the velocity field. We divide the measurement region into $m \times n = 32 \times 24$ (horizontal times vertical) grid cells and use a weighting function to interpolate the particles onto this grid. The weighting

function can be chosen in the DigImage program, and we use a weighting function defined to be $W_j^{(m,n)} = 1 - \frac{r_j}{R}$, where r_j is the distance from the center of grid cell (m, n) to particle j, and R is the weighting function length scale typically less than 4.5 cm (which is about 2.7 times the size of a grid cell). This means that particles with $r_j > R$ do not contribute to the velocity in that grid cell. Using this method we are able to achieve a relatively good measurement of the entire flow field, even in areas with few particles.

2.9 Visualization of the particle displacements

A question is how the particle positions computed by the software correspond to the physical particle movement. I an attempt to visualize this we have taken a sequence of 5 images (shown in figure 8) with a separation of 0.04 s, which is the period used to calculate a velocity vector. Figure 9-a) shows these images added together to display the particle displacement between the time steps, while figure 9-b) shows the corresponding positions as calculated by DigImage. Figure 10 shows a small subsample of the images from figure 8 and figure 11 shows the positions in the corresponding sub window, again a) visualized by adding the images together and b) DigImage calculations. We observe that we are only able to track a small amount of the particles present in the field due to large concentration at the pycnocline and also due to some particles being smaller than 3 pixels in area. The full images contain about 1600 traceable particles in this example, while in the sub sampled windows the computer tracks about 100 particles.

2.10 A note on accuracy and errors

There are a few errors associated with particle tracking that need to be addressed before we can turn to our results. First we need to know how closely the particles follow the fluid flow. A simple analysis of this can be found in Grue et al. (1998). They found for these experiments, that

$$\frac{|v - V|}{|V|_{\max}} \sim \frac{2R^2}{9\mu T} \sim 0.005 - 0.01,$$

where V is the particle velocity, v the fluid velocity and R the particle radius, assuming that $R = 0.5$ mm and $\mu = 10^{-6}\mathrm{m}^2\mathrm{s}^{-1}$. Thus, they concluded that the particles follow the fluid flow with an accuracy better than 1%. Second we turn to the particle tracking software and the question of how accurate it is in determining particle velocities. As mentioned in chapter 2.8.2 the error associated with determining the particle positions is estimated by Dalziel (1992) to be on the order of 0.2 pixels in his experiments. Grue et al. made an estimate of the error this introduces in the measured velocities by saying that this error is always better than 1 pixel and relating it to the maximal velocity in their measurements finding a relative error smaller than about 5%. Additional error sources do, however, exist such as inhomogeneities in the experimental setup, inhomogeneous particle seeding, local effect of surface tension at the free surface, incorrect pairing of particles and in some cases rather noisy images.

1) 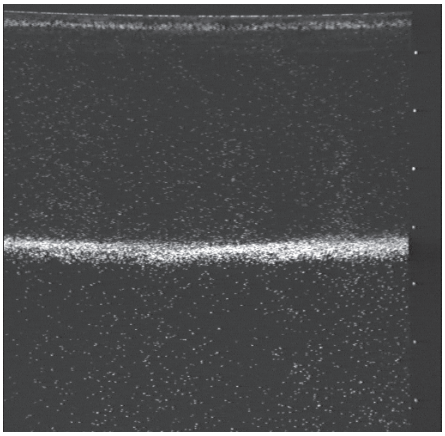 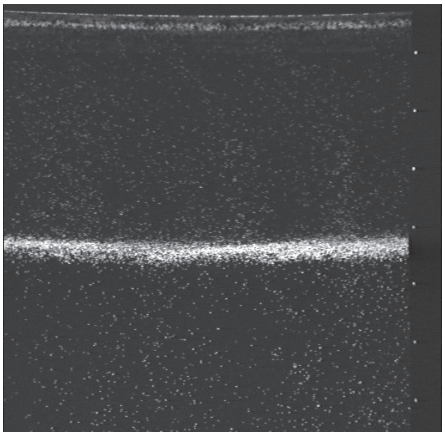 2)

3) 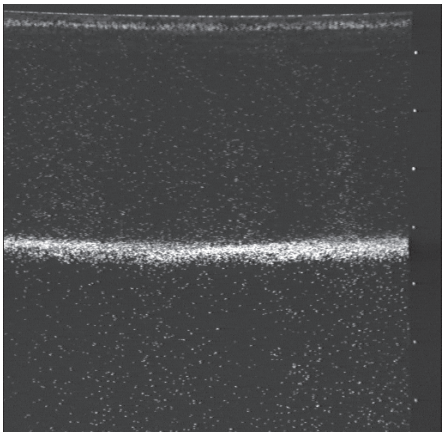 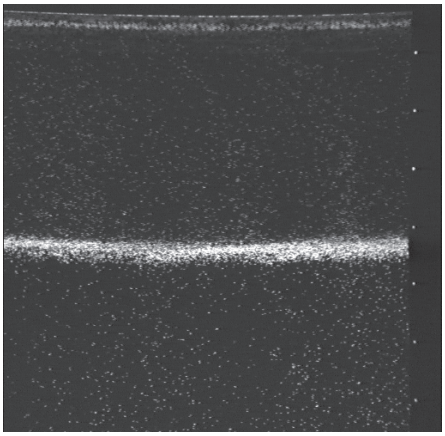 4)

5) 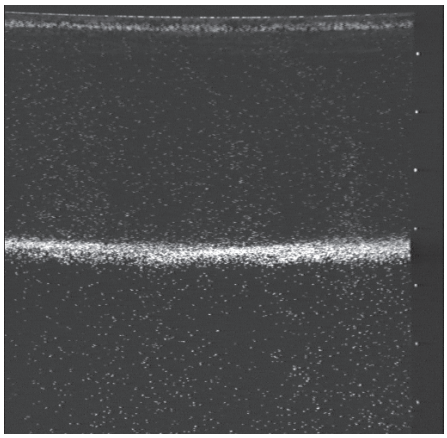

Figure 8: Images taken with $0.4s$ separation.

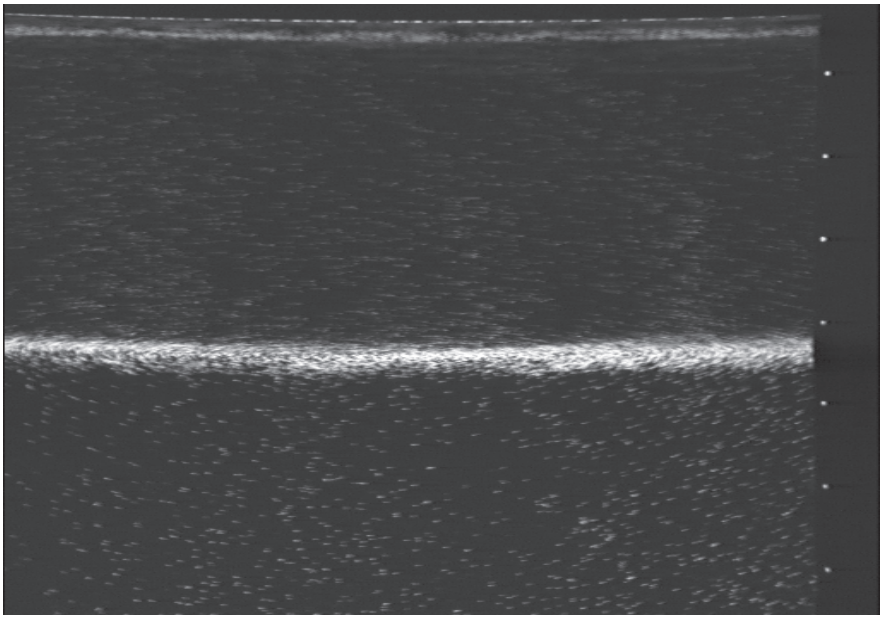

a)

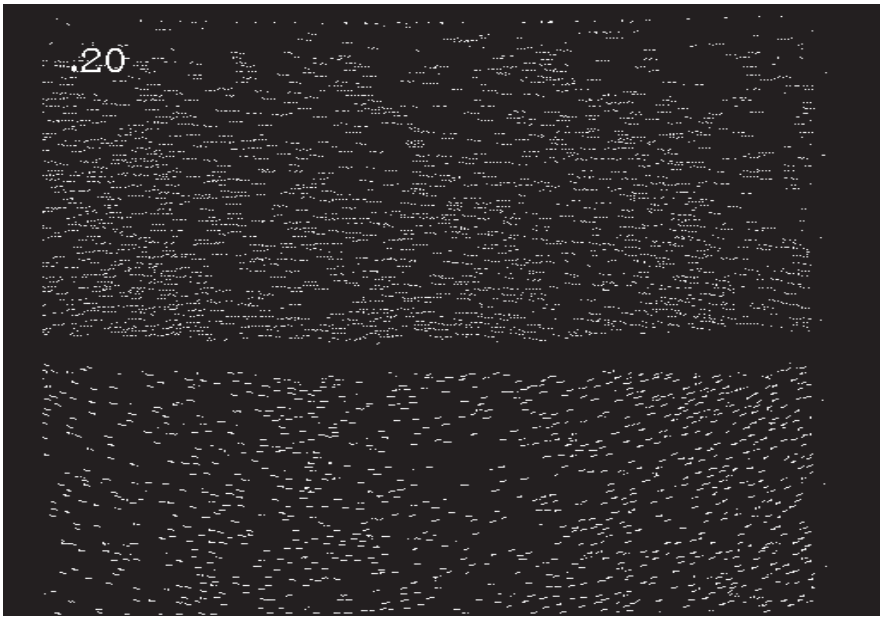

b)

Figure 9: a) Paths visualized by adding 5 images together and b) paths calculated by DigImage.

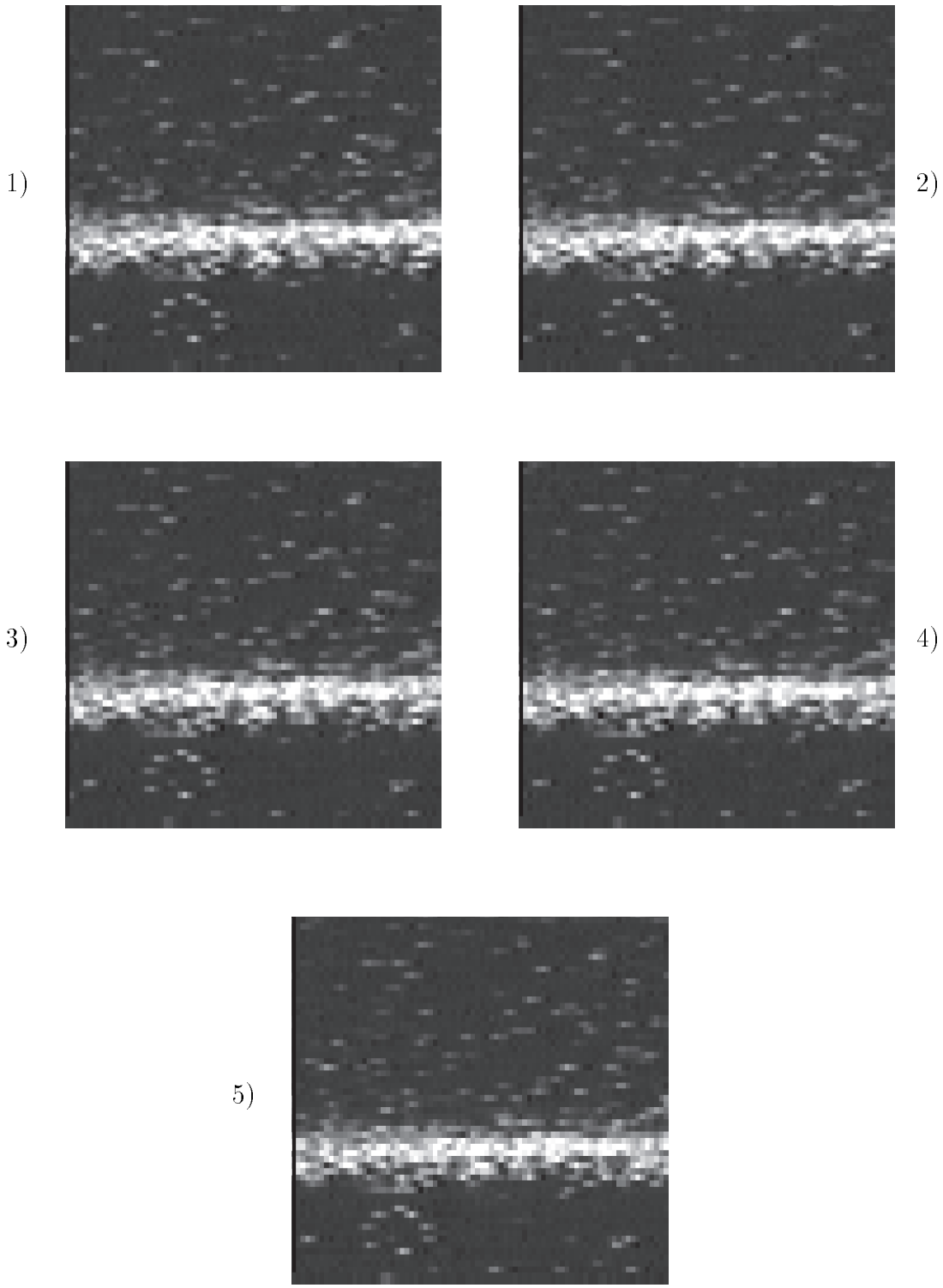

Figure 10: A small subsample of the full images taken with 0.4s separation.

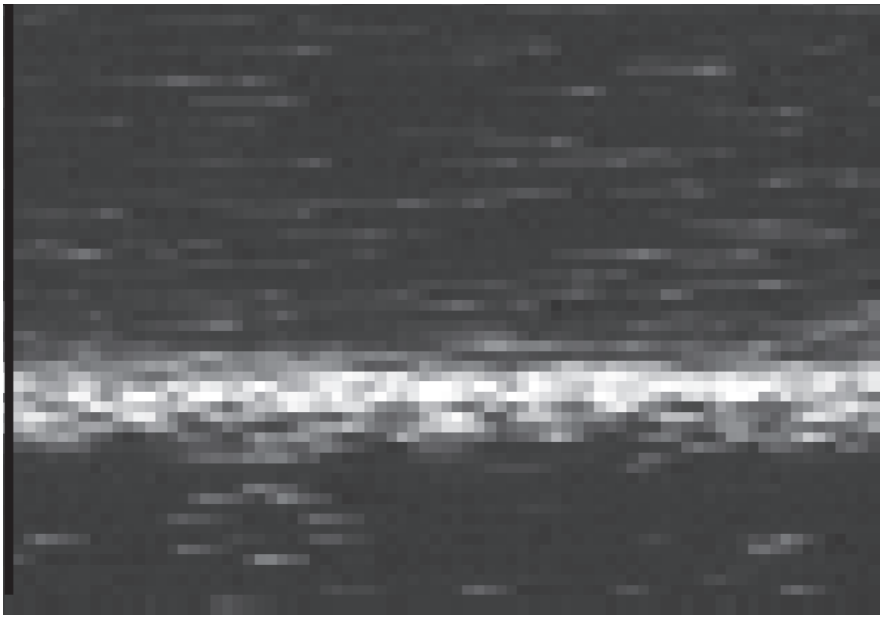

a)

b)

Figure 11: a) Paths in a sub window visualized by adding the images and b) as calculated by DigImage for the sub window specified.

3 Some results of the measurements

We here give some results of the experiments for illustration. Further result may be found in Grue et al. (1998).

3.1 Particle paths

Using the tracking data we are able to display the calculated particle paths and calculate the velocity fields using a program accompanying DigImage; Trk2DVel. Figure 12 shows the paths visualized by displaying the particle positions at several time steps with an intensity linearly decreasing as a function of time.

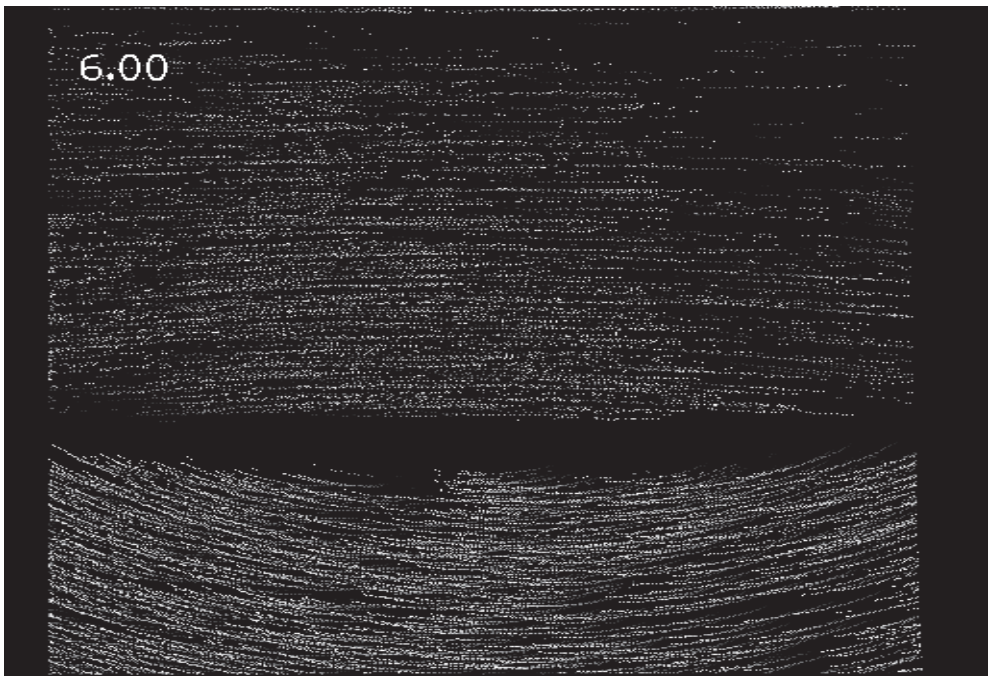

Figure 12: Particle paths as visualized by DigImage. The wave is moving from left to right in the picture.

3.2 Velocity fields in a two-layer model

Figure 13 shows a typical velocity field as measured in these experiments. We note that we in some measurements have small blank areas in the velocity field due to insufficient

particle seeding. This is also visualized in figure 12 which shows the corresponding paths used to calculate the velocities in figure 13.

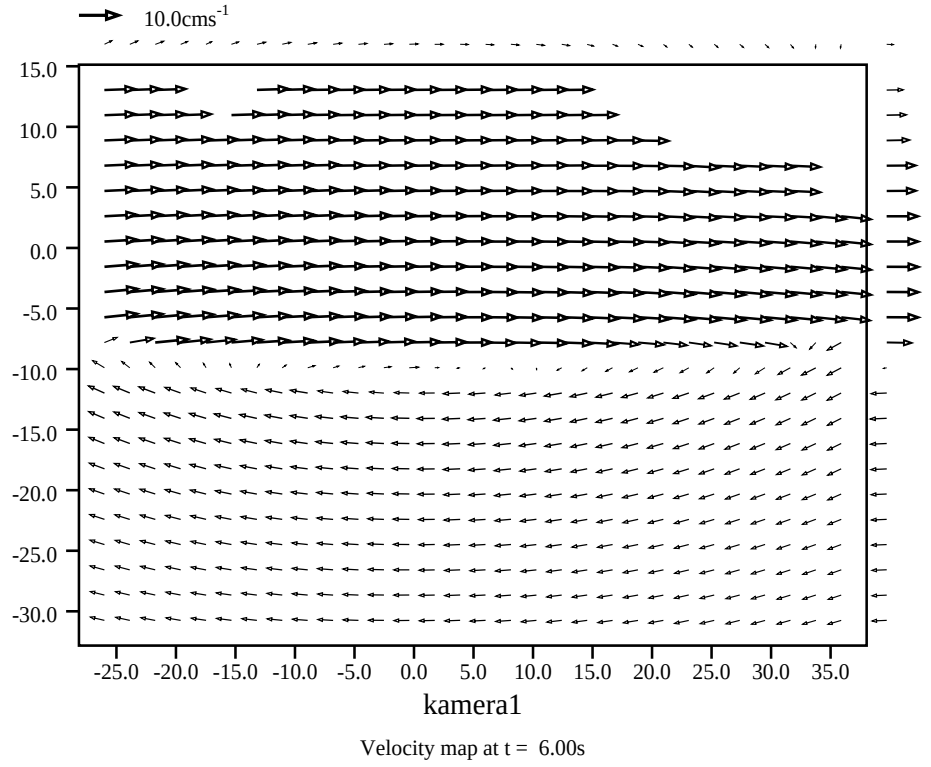

Figure 13: Typical velocity field in a two layer model. The wave is moving from left to right.

3.2.1 Horizontal velocity at the crest

To compare the experimental results with existing theory we have chosen to use the horizontal velocity at the crest of the wave, as this parameter includes the largest velocity values in the field. Figure 14 shows the experimental values taken from 10 different experiments with approximately equal initial conditions. These are:

- Initial volume, $V = 65\text{dm}^3$,
- $h_1 = 62$ cm,
- $h_2 = 15$ cm and
- Nondimensional amplitude, $a = \frac{a_{\text{exp}}}{h_2} \approx 0.78$.

We observe an excellent agreement between theory and experiments. The depth in the figure is made nondimensional with respect to the thickness of the upper layer, h_2, while the horizontal velocity, u, is made nondimensional with respect to the linear long wave speed c_0, given by

$$c_0^2 = \frac{gh_1h_2(\rho_1 - \rho_2)}{\rho_2(h_1 + h_2)}.$$

This is done to remove the effects of the small variations in ρ_1 and ρ_2 from experiment to experiment.

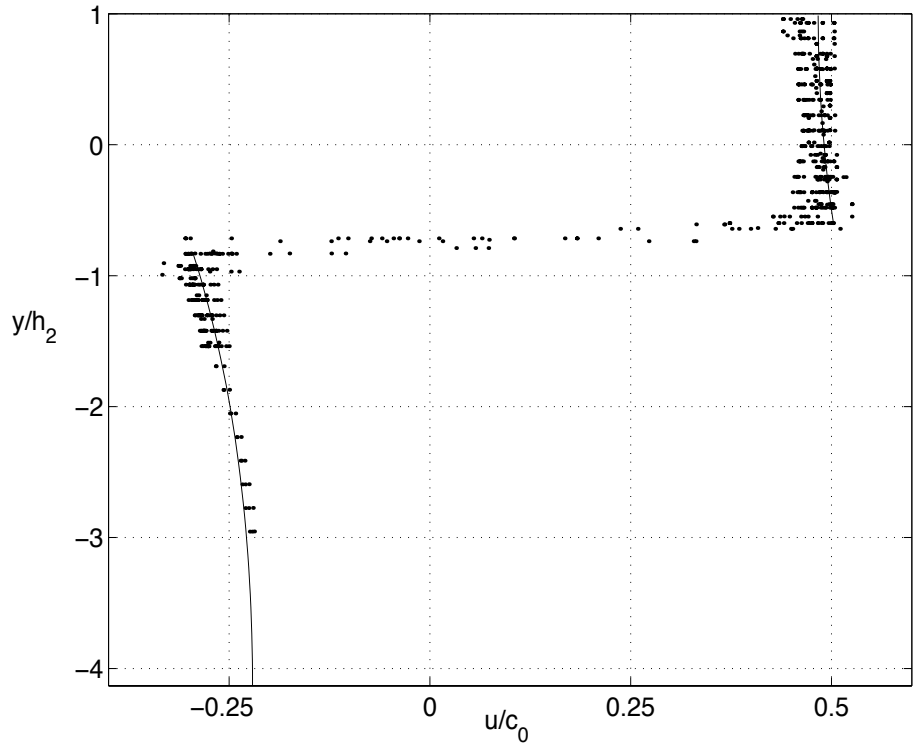

Figure 14: Horizontal velocities measured at the crest. Solid line: fully nonlinear theory. Dots: measurements.

Figure 15 presents 4 different conductivity measurements taken from experiments included in figure 14. We have performed experiments with some variation in the pycnocline thickness. The measurements show, however, that the pycnocline thickness has relatively small effect on the induced velocities in the fluid.

3.3 Measurements of propagation velocity c

Measurements of propagation velocities can be done simply by dividing the distance, Δx, between the two measuring positions with the time, Δt. In all our measurements Δx is

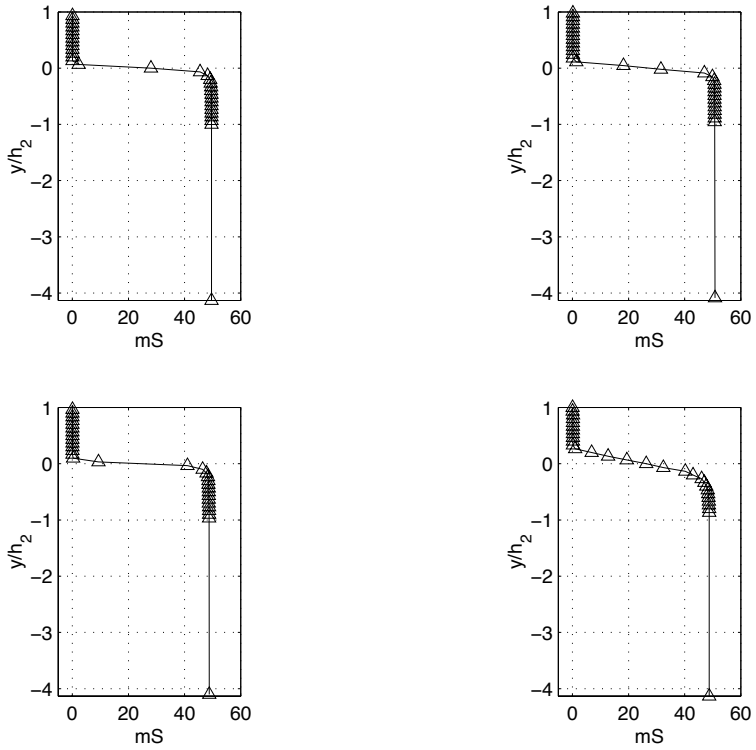

Figure 15: Initial conductivity profiles measured from 4 of the 10 experiments presented in figure 14.

about 6 m while Δt is at about $30 - 40$ s, the latter depending on the propagation speed. We have chosen to compare our measurements with weakly nonlinear KdV-theory and fully nonlinear theory (see Grue et al. (1998)).

It is worth noticing that the velocity that we measure is the velocity of a wave with an amplitude that is the mean of the two measuring positions (which is the two cameras). The differences in amplitude between the two positions is illustrated as horizontal bars in figure 16 together with the results. In this figure the x-axis (amplitude) is made nondimensional with respect to h_2 and the y-axis (speed) is made nondimensional with respect to c_0. To find ΔX we first determine the vertical position of the pycnocline, when the slope is maximal, at a given horizontal position, X_{or1}, at the first camera. This is followed by locating the same vertical value for the pycnocline in camera no. 2 and then determining the accompanying horizontal value, X_{or2}. Then Δx is found by

$$\Delta x = -X_{\mathrm{or1}} + X_{\mathrm{ref1}} + X_{\mathrm{ref1toref2}} - X_{\mathrm{ref2}} + X_{\mathrm{or2}},$$

where X_{or1} and X_{or2} are measured in local coordinates, X_{ref1} is the distance from the origin to the reference point in the first frame, $X_{\mathrm{ref1toref2}} = 5.927$ m is the distance between the reference points in the two frames and X_{ref2} is the distance from the origin to the reference point in the second frame.

3.3.1 Errors associated with the propagation velocity calculations

The software program DigImage allows us to control and grab images with exact timing. This means that the only errors introduced in these calculations are associated with determining Δx. This quantity is approximately determined by the thickness of the pycnocline divided by it's slope times Δt, implying a larger error for waves with small amplitude, where the slope is small.

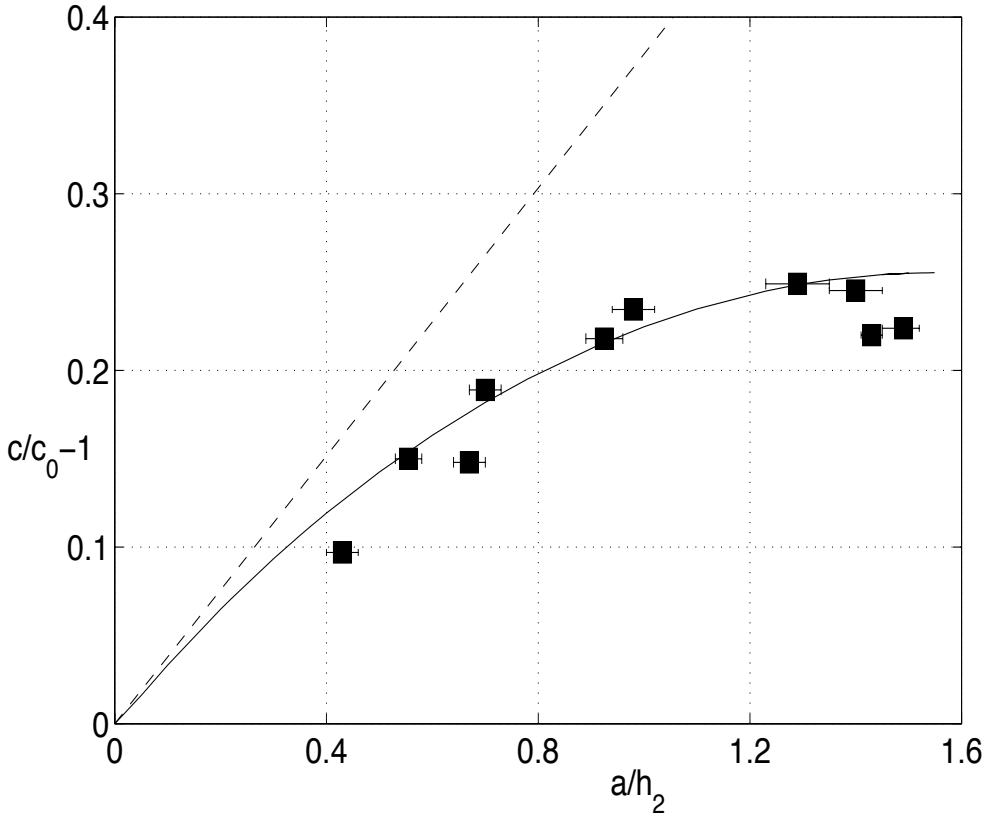

Figure 16: Measurements of propagation velocities with $\frac{c}{c_0} - 1$ on the vertical axis and $\frac{a}{h_2}$ on the horizontal axis. Solid line: fully nonlinear theory. Dashed line: KdV theory. Squares: measurements. Horizontal bars indicate amplitude reduction between recording sections.

4 Conclusion

In this paper we have experimentally investigated internal waves in a two-layered fluid with the object of obtaining reliable measurement methods applicable to internal waves and then to measure quantities such as velocity fields, propagation speed and wave shape. We use fresh water above salt water with a depth ratio between the layers of 4.13. The pycnocline is in most cases about 0.13 times the thickness of the upper layer, but in some experiments we also use a pycnocline of about 0.26.

The main purpose of this paper is to complement the paper by Grue et al. (1998) and provide a full description of the experimental method and setup. We have included a few results for visualization purposes, but a complete presentation of the results is found in the article mentioned above.

We apply Particle Tracking Velocimetry (PTV) to measure the velocity fields and basic image analysis to measure propagation speed and wave shapes. We find that the particle tracking routine in general is very suitable to these experiments as the velocities and, more important, the accelerations induced by the waves are relatively small. We also find that the method for determining the propagation velocity and wave shape is robust and accurate, although simple.

These measurements have been compared with a fully non-linear theory, finding a striking agreement for all amplitudes and all quantities measured, even when the pycnocline is relatively thick. In figure 14 we show the results of ten different experiment runs with approximately equal initial conditions. This figure also visualizes, to some extent, the accuracy of the measurements. The error in the measured velocities nondimensionalized by the linear long wave speed is less than 7-8%.

The authors wish to thank Mr. Arve Kvalheim and Mr. Svein Vesterby for their skillful technical assistance. This work was conducted under the Strategic University Programme 'General Analysis of Realistic Ocean Waves' funded by the Research Council of Norway.

References

[1] R. J. Adrian: "Particle-imaging techniques for experimental fluid mechanics", *Annu. Rev. Fluid Mech,* **23**: 261-304, 1991.

[2] J. Apel, J. Holbrook, A. K.Liu og J. J. Tsai: "The Sulu Sea Internal Soliton Experiment". *J. Phys. Oceanography,* **15**: 1625-1651, 1985.

[3] T. B. Benjamin: "Internal waves of permanent form in fluids of great depth". *J. Fluid Mech,* **29**,3: 559-592, 1967

[4] S. B. Dalziel: "Decay of rotating turbulence: some particle tracking experiments". *Applied Scientific Research,* **49**: 217-244, 1992.

[5] S. B. Dalziel: "Raleigh-Taylor instability: experiments with image analysis". *Dynamics of Atmospheres and Oceans,* **20**: 127-153, 1993.

[6] M. J. Drayton: "Eulerian and Lagrangian studies of inhomogeneous turbulence generated by an oscillating grid". *PhD-thesis,* DAMTP, University of Cambridge, 154 pages.

[7] B. Gjevik og S. E. Høst: "Langkammede indre bølger i Skagerak". *Naturen,* **6**: 209-214, 1984. (In norwegian).

[8] J.Grue, H. A. Friis, E. Palm og P. O. Rusås: "A method for computing unsteady fully nonlinear interfacial waves". *J. Fluid Mech,* **351**: 223-252, 1997.

[9] J.Grue, A. Jensen, P. O. Rusås and J. K. Sveen: "Properties of large amplitude internal waves". *University of Oslo, Preprint series,* 1998. Submitted for publication.

[10] Hichcock F.L. The distribution of a product from several sources to numerous localities. *J. Math. Phys*, **20**, 1941.

[11] T. Kao, F. Pan og D. Renouard: "Internal solitons on the pycnocline: generation, propagation, and shoaling and breaking over a slope". *J. Fluid Mech,* **159**: 19-53, 1985.

[12] G. H. Keulegan: "Characteristics of Internal Solitary Waves". *J. Research of the National Bureau of Standards,* **51,3**: 133-140, 1953.

[13] C. G. Koop and G. Butler: "An investigation of internal solitary waves in a two-fluid system". *J. Fluid Mech,***112**: 225-251, 1981.

[14] R. R. Long: "Solitary Waves in the One- and Two-Fluid Systems". *Tellus,* 8: 460-471, 1956.

[15] R. C. Weast (editor): "Handbook of Chemistry and Physics". *CRC Press*, 1974-1975.